Production of the most neutron-deficient Zn isotopes by projectile fragmentation of math xmlns="http://www.w3.org/1998/Math/MathML">mmultiscripts>mi>Kr/mi>mprescripts>/mprescripts>none>/none>mn>78/mn>/mmultiscripts>/math>

A. Kubiela et al.

Phys. Rev. C **104**, 064610 — Published 10 December 2021

DOI: 10.1103/PhysRevC.104.064610

Production of the most neutron-deficient Zn isotopes by projectile fragmentation of ^{78}Kr

A. Kubiela,[1,*] H. Suzuki,[2] O.B. Tarasov,[3] M. Pfützner,[1,†] D.-S. Ahn,[2] H. Baba,[2] A. Bezbakh,[4] A.A. Ciemny,[1] W. Dominik,[1] N. Fukuda,[2] A. Giska,[1] R. Grzywacz,[5] Y. Ichikawa,[2,6] Z. Janas,[1] Ł. Janiak,[7] G. Kamiński,[4,8] K. Kawata,[2,9] T. Kubo,[2] M. Madurga,[5] C. Mazzocchi,[1] H. Nishibata,[2,6] M. Pomorski,[1] Y. Shimizu,[2] N. Sokołowska,[1] D. Suzuki,[2] P. Szymkiewicz,[4,10] A. Świercz,[4,10] M. Tajima,[2] A. Takamine,[2] H. Takeda,[2] Y. Takeuchi,[2,11] C.R. Thornsberry,[5] H. Ueno,[2] H. Yamazaki,[2] R. Yokoyama,[5] and K. Yoshida[2]

[1]*Faculty of Physics, University of Warsaw, 02-093 Warszawa, Poland*
[2]*RIKEN Nishina Center, 2-1 Hirosawa, Wako, Saitama 351-0198, Japan*
[3]*National Superconducting Cyclotron Laboratory, Michigan State University, East Lansing, Michigan 48824, USA*
[4]*Flerov Laboratory of Nuclear Reactions, JINR, 141980 Dubna, Russia*
[5]*Department of Physics and Astronomy, University of Tennessee, Knoxville, Tennessee 37996, USA*
[6]*Department of Physics, Kyushu University, 744 Moto-oka, Nishi, Fukuoka, Fukuoka 819-0395, Japan*
[7]*National Centre for Nuclear Research, 05-400 Otwock, Świerk, Poland*
[8]*Heavy Ion Laboratory, University of Warsaw, 02-093 Warsaw, Poland*
[9]*Center for Nuclear Study, University of Tokyo, 7-3-1 Hongo, Bunkyo, Tokyo 113-0033, Japan*
[10]*AGH University of Science and Technology, Faculty of Physics and Applied Computer Science, 30-059 Krakow, Poland*
[11]*Department of Advanced Sciences, Hosei University*

(Dated: November 17, 2021)

The cross sections for the production of three most neutron-deficient zinc isotopes, $^{54-56}$Zn, in the projectile fragmentation of ^{78}Kr at 345 MeV/nucleon on a beryllium target, were measured. Although the results are smaller by over an order of magnitude from those obtained with ^{58}Ni beam at 75 MeV/nucleon on a nickel target, the rates of reaction products are found larger in the case of high-energy fragmentation of ^{78}Kr. The experimental cross sections for the most neutron-deficient isotopes of even-Z nuclei between zinc and krypton were analysed in the framework of the abrasion-ablation (AA) model. A very good agreement with the data was found when the nuclear masses predicted by a particular variant of the Hartree-Fock-Bogoliubov (HFB22) mass model were used. The prospects for the observation of more exotic isotopes in this region is discussed in context of 2p radioactivity.

I. INTRODUCTION

The study of nuclei at the limits of stability is currently one of the most important frontiers of nuclear physics. It provides crucial data for testing theoretical models helping to develop a unified understanding of nuclear properties and phenomena over large areas of nuclidic chart. Particularly interesting are nuclei at and beyond the proton drip-line. In contrast to the neutron rich edge of the chart, the proton drip-line can now be accessed experimentally for almost all elements below bismuth [1]. Very neutron-deficient nuclei display many characteristic features like β-delayed emission of charged particles or two-proton (2p) radioactivity [1, 2]. These decay modes provide valuable information on the nuclear structure in this region, while they also represent challenges to nuclear theory. On the other hand, the knowledge of properties of these nuclei is essential for the modelling of the astrophysical *rp*-process [3].

Two-proton radioactivity is the most recently discovered, and the least known, nuclear decay mode. It occurs for those unbound even-Z nuclei for which the single-proton separation energy is positive or very small [1, 2]. Measurement of the partial half-life for this process and the decay energy offer the first important data on a very exotic nucleus. A new and unique insight into its structure can be gained by the study of the correlations of momenta of the two protons emitted simultaneously from a nuclear ground state [1]. This information, however, is still scarce and limited to few cases [4]. The main obstacle is the difficulty in the production of 2p-decaying nuclei in amounts sufficient to carry out statistically significant correlations studies. From this perspective, it is important to identify the best production method for the nuclei of interest.

Here we focus on the region of even-Z nuclei at the proton drip-line between nickel and krypton. Three 2p-emitting nuclei are among them: ^{48}Ni [5], ^{54}Zn [6], and ^{67}Kr [7]. In addition, 2p radioactivity is predicted to occur also in isotopes of germanium, ^{57,58}Ge, and selenium, ^{62,63}Se [8, 9]. The ^{48}Ni and ^{54}Zn isotopes were discovered by means of projectile fragmentation of a ^{58}Ni beam on a natural nickel target [6, 10–13]. For the heavier cases, with atomic number $30 < Z < 36$, projectile fragmentation of ^{78}Kr is considered as the method of choice. Stolz et al. employed ^{78}Kr fragmentation on a beryllium target and the A1900 fragment separator at the NSCL-MSU laboratory and were the first to identify ^{60}Ge and ^{64}Se [14]. The production cross sections for five most neutron-deficient isotopes of germanium and selenium were determined in that work. Using the same reaction and the same separator Ciemny et al. produced ^{59}Ge for the first time and (re)measured production cross sections for $^{59-62}$Ge [15]. Recently, Blank et al. investigated production of proton drip-line nuclei by ^{78}Kr fragmentation using the BigRIPS separator at the RIKEN Nishina Center [16]. Three very exotic nuclei, ^{63}Se, ^{67}Kr, and ^{68}Kr were identified for the first time,

* adam.kubiela@fuw.edu.pl
† pfutzner@fuw.edu.pl

and the cross sections for the two most neutron-deficient isotopes of germanium, selenium, and krypton were determined, among other findings [16].

Motivated by the excellent performance of the BigRIPS separator, and in particular by the large intensity of the ^{78}Kr beam available at the RIKEN laboratory, we made an attempt to produce the 2p-decaying nucleus ^{54}Zn in ^{78}Kr fragmentation. Results of spectroscopic studies of this and neighboring nuclei will be presented in a separate publication. Here we report on the measurement of the production cross section for the three most exotic zinc isotopes, $^{54-56}$Zn. Furthermore, we compile the measured cross sections for the most neutron-deficient zinc, germanium, selenium, and krypton isotopes, and compare them with model predictions. Finally, we discuss prospects for the production of even more neutron-deficient isotopes in this region.

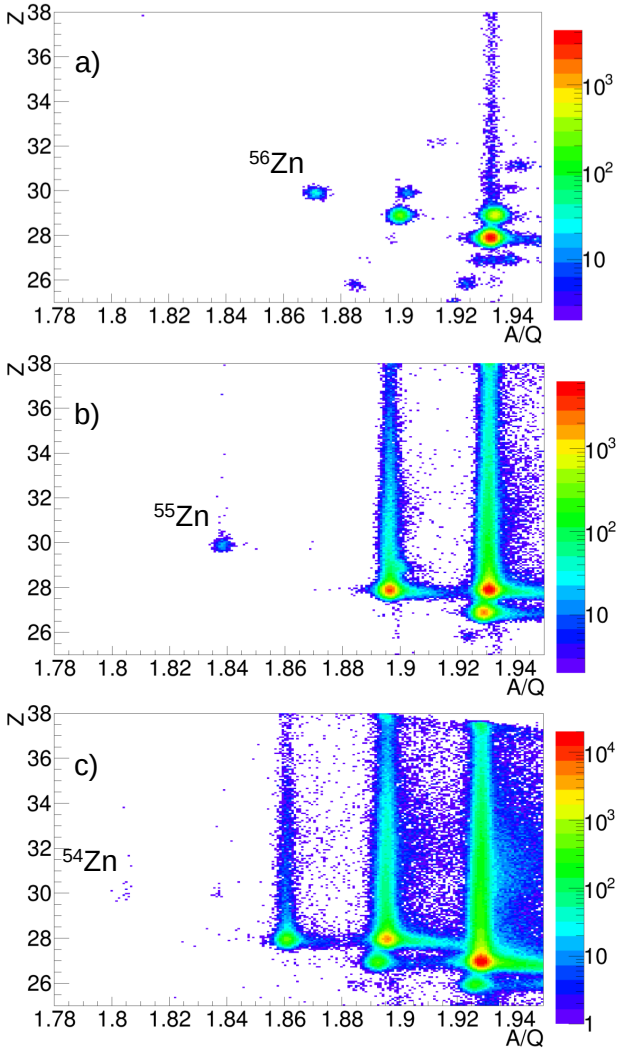

FIG. 1. (Color online) Particle identification plots showing the mass-to-charge ratio A/Q and the atomic number Z for the three zinc isotopes investigated. The plots for ^{56}Zn (a) and for ^{54}Zn (c) correspond to settings detailed in the second and the fourth row of Table I, respectively.

II. EXPERIMENT AND DATA ANALYSIS

The experiment was carried out at the RI Beam Factory (RIBF) of the RIKEN Nishina Center. The nuclei of interest were produced using a ^{78}Kr primary beam at 345 MeV/nucleon impinging on a 10 mm-thick beryllium target and separated with the help of the large-acceptance two-stage fragment separator BigRIPS [17, 18]. Two aluminum wedge-shaped degraders were used: 4 mm-thick and 1.5 mm-thick at the momentum dispersive focal planes F1 and F5, respectively. Ions coming to the final focal plane of the separator (F7) were identified in flight by a set of standard BigRIPS detectors and the ΔE-TOF-$B\rho$ method [19]. The time of flight (TOF) was measured by two 500 μm thick plastic scintillators mounted at the achromatic foci F3 and F7. The magnetic rigidity ($B\rho$) was determined from particle tracking information provided by a set of position sensitive parallel plate avalanche counters (PPAC) located at F3, F5, and F7 focal planes. The energy loss (ΔE) was measured with the help of the ionization chamber placed at the F7 focus.

Data were collected using three main settings of the separator, optimized for the transmission of ^{56}Zn, ^{55}Zn, and ^{54}Zn, respectively. For the cases of ^{56}Zn and ^{54}Zn, two variants of the setting with slightly different opening of the F2 slit were used. The relevant parameters of these settings are collected in Table I. The average beam current was varying from about 8 pnA for ^{56}Zn to about 240 pnA for ^{54}Zn.

The particle identification plots used to select and count the number of ions of interest are presented in Figure 1. The data analysis was performed following the methods described in Ref. [19]. In particular, a background removal procedure utilizing the charge and the time information from the left and right readouts of the plastic scintillators mounted at F3 and F7, was applied [19]. Due to the large beam intensity and the large target thickness, pile-up effects were observed in the ΔE and in the TOF signals, affecting the determination of the atomic number Z and the mass-to-charge ratio A/Q, respectively, as can be seen in Figure 1. The zinc isotopes of interest were well isolated from other ions in the identification plots, which allowed to count the events due to pile-up. Since the adopted background removal procedures [19] reduce also the number of good ions and pile-up events in the final identification plot, we have carefully determined the magnitude of these effect. The final number of ions of interest, given in Table I, takes into account pile-up events and includes small corrections compensating for the losses due to the purification procedures.

The production cross-section σ is determined using the formula:

$$\sigma = \frac{N_{\mathrm{Zn}}}{N_{\mathrm{beam}}} \frac{A}{d\, N_A\, T\, \eta}, \qquad (1)$$

where N_{Zn} is the number of observed zinc ions, N_{beam} is the number of beam particles impinging on the target, A is the molar weight of the target, d is the areal target thickness, N_A is the Avogadro number, T is the transmission through BigRIPS, and η is the efficiency of the data acquisition system. The number of projectiles hitting the target N_{beam} was mea-

TABLE I. Details of the experimental settings used in the experiment. For each of them the irradiation time, the primary beam dose (N_{beam}), the F2 slit positions, the transmission through the BigRIPS separator up to F7 (T), the efficiency of the acquisition system (η), and the deduced number of ions of interest (N_{Zn}) are given. The setting of the F1 slit was the same in all cases and amounted to +64.2/-42.8 mm. See text for details.

Setting	Time [h]	N_{beam}	F2 slit [mm]	T [%]	η [%]	N_{Zn}
^{56}Zn	1.3	$(22.7 \pm 3.7) \times 10^{13}$	6.0/-6.0	66.8	70.5	398 ± 20
^{56}Zn	2.06	$(59.2 \pm 9.6) \times 10^{13}$	3.0/-6.0	58.8	57.4	783 ± 28
^{55}Zn	6.2	$(36.3 \pm 6.9) \times 10^{15}$	3.0/-6.0	57	37.1	838 ± 32
^{54}Zn	25.2	$(12.29 \pm 0.93) \times 10^{16}$	6.0/-6.0	65	52.2	21 ± 5
^{54}Zn	13.4	$(71 \pm 13) \times 10^{15}$	5.0/-7.0	64	47.0	6 ± 5

sured with scattered beam particles by means of scintillation detectors located near the target. This system was calibrated three times during the experiment. Differences between the calibrations were used to estimate the uncertainty of the beam intensity which amounted to about 16%. The transmission T was determined with LISE^{++} ion-optical simulations [20]. This value takes into account the probability that the selected ion is destroyed in a secondary reaction in any layer of matter it passes through, including the production target. The uncertainty of the transmission was estimated by varying the LISE^{++} simulation settings while keeping the position distribution of ions at F3, F5, and F7 foci consistent with the observations. Finally, we have adopted for this uncertainty a rather conservative value of 30% which dominates the final systematical error of the measured cross sections. The efficiency of the acquisition system η was determined from the ratio of accepted triggers to all triggers registered during the run by dedicated scalers.

III. RESULTS AND DISCUSSION

Using Eq. (1) production cross sections were determined for each setting listed in Table I. The measurements for ^{56}Zn and ^{54}Zn were done twice using slightly different settings. For both isotopes, the two variants yielded results consistent within error bars. Then, the final values for these isotopes were calculated by combining statistics obtained in the two variants. The determined production cross sections for zinc isotopes investigated in this work are presented in Table II and they are plotted in Figure 2. We find that the production of ^{54}Zn – the main goal of this experiment – occurs in the fragmentation of ^{78}Kr with a cross section of 3.5 fb. This nucleus was discovered at LISE3 separator at GANIL using the ^{58}Ni beam at 74.5 MeV/nucleon impinging on a 250 mg/cm^2 thick natural nickel target [6] with a production cross section of about 100 fb, thus by a factor of about 30 larger. Similarly, ^{55}Zn and ^{56}Zn were discovered at GANIL using the same reaction [21] and the determined cross sections were larger from those in our work by a factor of 23 and 17, respectively. For comparison, the results obtained at GANIL with the ^{58}Ni beam are also listed in Table II.

The production of the most neutron-deficient zinc isotopes using the ^{58}Ni beam at 75 MeV/nucleon on a nickel target occurs with the cross section larger by over an order of magnitude than in the fragmentation of ^{78}Kr at 345 MeV/nucleon on a beryllium target. Note that in the former reaction a pick-up of two protons must take place to create zinc from nickel. Presumably, due to the lower energy of the primary beam and the heavy target, other reactions channels, like a multi-nucleon transfer, contribute substantially to the reaction process which, in consequence, cannot be considered as a pure projectile fragmentation any more.

The final rate of produced nuclei, however, depends also on experimental conditions (luminosity), which in our case is the beam intensity, and the target material and its thickness. We compare the two production methods for ^{54}Zn making use of Eq. (1) again and neglecting the transmission and the acquisition dead time. Moreover, we assume the maximal beam intensity offered by the laboratories considered. The results are collected in Table III. It can be seen that the production rate of ^{54}Zn, using the conditions available at RIKEN, is larger by a factor of 3 than that at GANIL. The advantage of our approach is even greater if we take into account the transmission through the separator which is of the order of 10% for the LISE3 separator while it is typically above 50% for BigRIPS. The main factor in favor of the reaction used in this work is the much thicker target made of lighter material, which overcomes the lower production cross section. We conclude that the high-energy fragmentation of ^{78}Kr on a beryllium target is more effective method for the production of the most neutron-deficient zinc isotopes than the low-energy quasi-fragmentation of ^{58}Ni on a nickel target. In this context, it would be very interesting to verify how these cross sections change with the energy of the ^{58}Ni beam and with the target material.

In Figure 2, in addition to the experimental values obtained in this work, also the results from Refs. [14–16] are shown. Three model predictions are presented for comparison. The dotted (black) lines represent the EPAX3 empirical parametrization [22]. As was already noted before [16], in this region of nuclei the EPAX3 model overestimates the measured cross sections by a large factor, up to two orders of magnitude. This discrepancy is actually increasing when going away from stability, so this model should not be used for planning experiments aimed at more exotic neutron-deficient isotopes.

The solid (red) and dashed (brown) lines in Figure 2 show predictions obtained with the Geometrical LISE^{++} Abrasion-Ablation (AA) model [23]. In this model the fragmentation

TABLE II. Cross sections (in barns) for the production of most neutron deficient zinc isotopes. The columns 2-4 refer to the fragmentation of ^{78}Kr beam on a beryllium target used in the present work. The experimental values are compared to the predictions of the EPAX3 parametrization [22], and the AA model using the HBF22 mass predictions [39], see text for details. The last column shows the production cross sections measured for the ^{58}Ni beam at 74.5 MeV/nucleon on a natural nickel target, reported in Refs. [6, 21].

Nucleus	σ_{exp}	σ_{EPAX3}	σ_{AA}	σ_{Ni}
^{56}Zn	$(3.1 \pm 0.1_{(stat)} \pm 1.0_{(syst)}) \times 10^{-11}$	8.45×10^{-11}	1.6×10^{-11}	$5^{+20}_{-2} \times 10^{-10}$
^{55}Zn	$(8.8 \pm 0.3_{(stat)} \pm 3.1_{(syst)}) \times 10^{-13}$	3.47×10^{-12}	3.8×10^{-13}	$2.0^{+0.6}_{-0.5} \times 10^{-11}$
^{54}Zn	$(3.5 \pm 0.7_{(stat)} \pm 1.2_{(syst)}) \times 10^{-15}$	1.47×10^{-13}	4.1×10^{-15}	$\approx 1 \times 10^{-13}$

TABLE III. Comparison of the two reactions used to produce ^{54}Zn at RIKEN and at GANIL. For each laboratory the primary beam is given, its energy (E) and intensity (I), the production target material and its thickness (d), the cross section, and the production rate at the target (Y).

Lab	Beam	E [MeV/u]	I [pnA]	Target	d [g/cm^2]	σ [fb]	Y [1/day]
GANIL	^{58}Ni^{+26}	75	154	Ni	0.250	100	22
RIKEN	^{78}Kr^{+36}	345	300	Be	1.850	3.5	70

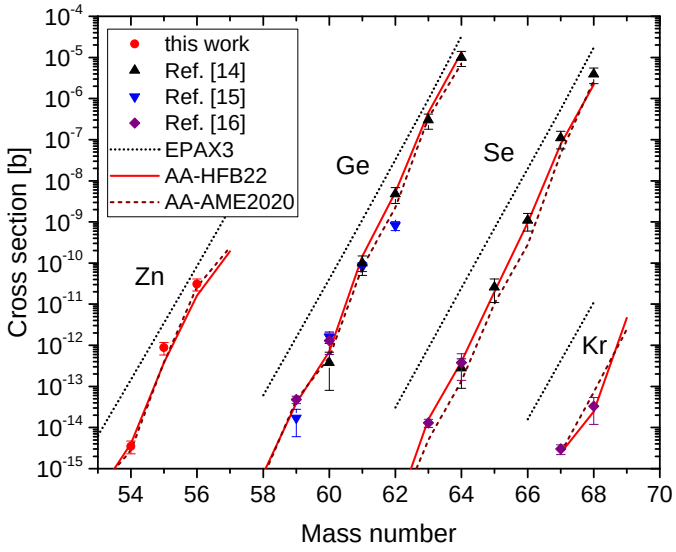

FIG. 2. (Color online) Measured production cross sections for the isotopes of zinc, germanium, selenium, and krypton in the fragmentation of ^{78}Kr, compared to predictions of the EPAX3 parametrization [22] and the AA model using the HFB22 mass model [39] and the AME2020 mass tables [34].

reaction proceeds in two steps. The first, abrasion process accounts for removal of nuclear matter in the overlap region of the colliding ions [24]. The excitation energy due to surface distortion of the projectile prefragment, following abrasion of nucleons, is calculated from the clean-cut abrasion formalism [25]. Modeling of the second step, ablation, is based on the fusion–evaporation model LisFus [26]. It employs fast analytical calculation of fusion residues cross sections. The evaporation stage is treated in a macroscopic way using a master equation which leads to diffusion equations as proposed by Campi and Hüfner [27], and reexamined later by Gaimard and Schmidt [28]. Level densities and decay widths are taken from the statistical analysis of Iljinov et al. [29]. The LISE evaporation model initially took into account eight possible channels (n, 2n, p, 2p, d, t, ^{3}He, α), later also fission and breakup de-excitation channels were implemented [30]. An analytical solution of the evaporation cascade was performed with the transport integral method [31] providing fast calculations and allowing cross section determination for nuclei far from stability, which are not accessible with the Monte Carlo technique.

The new minimization utility, recently implemented in the LISE code, allows to deduce the AA model parameters using experimental cross-sections. It is based on the the Levenberg–Marquardt nonlinear least square algorithm, implemented in the `levmar` package [32]. Six parameters of the AA model are determined in this way. Four of them are used to characterize the excitation energy of the prefragment created in the abrasion phase of the reaction. The distribution of this energy is approximated by a Gaussian function [28]. Both the centroid and the standard deviation of this function are described by a second order polynomial of the type $a\Delta A + b\Delta A^2$, where ΔA is the number of abraded nucleons, and a and b are fitted parameters. The fifth parameter is related to the effective Coulomb barrier and the final one is an overall normalization factor. In addition, the important input to the AA model is the table of masses of all nuclei in the region between the projectile and the fragments of interest. In the analysis we have considered 11 mass models: AME2016 [33] and AME2020 [34] mass tables, the TUYY and KTUY empirical mass formulas [35, 36], the finite-range droplet (FRDM12) [37], the Weizsäcker-Skyrme (WS4 and WS4$_{\rm RBF}$) [38] microscopic-macroscopic mass formulae, two versions of the nonrelativistic Hartree-Fock-Bogoliubov model (HFB22, HFB27) [39, 40], and two energy density functional (EDF) models based on UNEDF0 [41] and UNEDF1 [42] functionals. For each mass model, a minimization procedure was executed to find the parameters of the AA model best fitting the measured cross sections for 17 nuclei shown in Figure 2. The best results were found for the HFB22 model [40] and

TABLE IV. Production cross section in ^{78}Kr fragmentation (σ), one- (S_p) and two-proton (S_{2p}) separation energies according to HFB22 mass model [39], and the partial half-life for two-proton emission ($T^{2p}_{1/2}$) estimated with the direct model [8]. The cross section values for ^{58}Ge and ^{62}Se are predicted by the AA model in this work. See text for details.

Nucleus	σ [barn]	S_p [MeV]	S_{2p} [MeV]	$T^{2p}_{1/2}$
^{59}Ge	$(4.8 \pm 1) \times 10^{-14}$ [a]	0.349	-0.742	10^{11} s
^{58}Ge	7.6×10^{-16}	0.299	-2.122	0.6 μs
^{63}Se	$(1.3 \pm 0.3) \times 10^{-14}$ [a]	0.589	-1.512	1 s
^{62}Se	8.4×10^{-17}	0.099	-2.612	14 ns

[a] experimental value from Ref. [16].

these are shown in Table II and in Figure 2. Similar, albeit slightly worse, results were obtained for the AME2016 and WS4$_{\rm RBF}$ mass models. For comparison, we plot in Figure 2 also the results obtained for the newest mass table, based on experimentally measured masses, AME2020. The global fit for this model was a bit worse than for the AME2016 and HFB22 models. We note that with the HFB22 model fit, the excitation energy of the prefragment is given by $E^* = 13.3\,\mathrm{MeV}\ \Delta\mathrm{A} - 0.15\,\mathrm{MeV}\ \Delta\mathrm{A}^2$. The average from all mass models, weighted by the reduced χ^2 values, yielded the parameter values of 13.0 ± 0.5 MeV and -0.15 ± 0.14 MeV for the linear and the quadratic term, respectively.

As can be seen in Figure 2, the AA model with the masses predicted by the HFB22 theory describes very well the measured cross sections in the region considered here. Thus the AA-HFB22 model can be used to predict the production cross sections for more exotic isotopes. When considering the more neutron-deficient isotopes between zinc and krypton, we have to take into account that these are unbound nuclei, predicted to be ground-state two-proton emitters. In addition to the production cross section, the decay half-life is a crucial factor for the possibility to observe such a nucleus at the end of the fragment separator after a time-of-flight of the order of few hundreds of nanoseconds. For the rough estimate of the partial half-life for 2p emission here we use a simple direct model, described in Refs. [8, 43]. This model was tuned to obtain a reasonable agreement with the measured half-lives of the then-known cases of 2p radioactivity (^{19}Mg, ^{45}Fe, ^{48}Ni, and ^{54}Zn). First, we note that since ^{54}Zn and ^{67}Kr are established 2p-emitters, their more neutron deficient isotopes, ^{53}Zn and ^{66}Kr, respectively, will be less bound and thus undergoing proton emission with shorter half-life. Using the HFB22 mass model, their half-lives predicted by the direct model will be of the order of 10 ns. This will be the limiting factor for the decay study of these nuclei in projectile fragmentation experiments. The case of germanium and selenium isotopes is presented in Table III. The most neutron-deficient isotope of germanium observed to date, ^{59}Ge, fulfills the energy criteria for 2p radioactivity, but it is not sufficiently 2p-unbound to compete with β^+ decay. The most exotic selenium isotope known, ^{63}Se, also could decay by 2p emission with a partial half-life of the order of 1 s, which is much larger than the measured half-life for this nucleus, 13.2 ms [7]. In Ref. [7] no evidence for 2p radioactivity of ^{59}Ge and ^{63}Se was found, but it seems that a tiny branching, of the order of 1%, for 2p decay in the latter nucleus cannot be excluded. While ^{59}Ge is not sufficiently unbound for the observation of 2p emission, ^{58}Ge could be a more favourite case since its estimated half-life is of the order of a few hundreds of nanoseconds. The production cross section, according to our AA-HFB22 prediction, is 0.76 fb. The weighted average of this cross sections, from all mass models considered, is $0.7^{+0.6}_{-0.3}$ fb. Such a value will be within experimental reach of the upcoming fragmentation facilities like FRIB or FAIR.

Unfortunately, in the experiment reported in Ref. [16], no trace of ^{58}Ge was found and the cross section limit of 0.076 fb was estimated assuming one count observed. The authors of Ref. [16], using the yield systematics, expected about 20 counts of ^{58}Ge and from this they inferred a half-life limit of 100 ns for this nucleus. If we assume the cross section of 0.76 fb, as predicted by our AA-HFB22 prediction, we would expect 10 counts of ^{58}Ge in the conditions of Ref. [16]. With this number the half-life limit for ^{58}Ge would be 130 ns. In any case, it appears that ^{58}Ge decays faster than our rough estimate and this nucleus does not survive the flight through the BigRIPS.

The case of ^{62}Se is even less promising. Its estimated 2p-decay half-life is of the order of 10 ns, too short for a fragmentation experiment. In addition, its production cross section is predicted to be 8.4×10^{-2} fb (HFB22 mass model) or $6^{+5}_{-3} \times 10^{-2}$ fb (weighted average of all mass models). These values agree with the cross section limit of 0.081 fb deduced for ^{62}Se in Ref. [16]. This level of the cross section seems to be too small for the production method discussed here.

IV. SUMMARY

Using projectile fragmentation of a ^{78}Kr beam at the energy of 345 MeV/nucleon on a beryllium target, we have produced the three most neutron-deficient zinc isotopes known ^{56}Zn, ^{55}Zn, and ^{54}Zn and we have determined their production cross sections. The main nucleus of interest, ^{54}Zn, which is known to decay by 2p radioactivity [6] resulted to have the very low production cross section of 3.5 fb. Still, our production method is more effective than using a Ni beam at energy below 100 MeV/nucleon on a nickel target, for which the production cross section was estimated to be larger by a factor of 30 [6]. The main advantage of the fragmentation reaction at higher energy is the possibility to use a thicker target. For ^{54}Zn the total production gain due to the thick beryllium target used in our experiment over the thin nickel target used in Ref. [6] is given by a factor of about 3. The same conclusion, even to larger extent, is valid for ^{55}Zn and ^{56}Zn. The very interesting question arises how the cross sections discussed would change with increasing energy of the ^{58}Ni beam and for lighter targets.

We compared the measured cross section values, together with literature data available for the most-neutron deficient even-Z isotopes of germanium, selenium, and kryp-

ton, with theoretical predictions. We confirm that the EPAX3 parametrization [22] largely overestimates the experimental values and fails to serve as a guide for more exotic, neutron-deficient cases. On the other hand, the analysis in the frame of the abrasion-ablation (AA) model [23], leads to a very good agreement of the predicted cross sections with the data. An important ingredient in the AA model is the proper description of masses of all nuclei between the projectile and fragment of interest. The best results were found for one of the versions of the Hartree-Fock-Bogoliubov mass model (HFB22) [39].

Using the LISE^{++} AA model together with the HFB22 mass table, we have predicted the cross sections for more neutron deficient germanium and selenium isotopes, which may be interesting in the context of 2p radioactivity. For selenium we found that while a very small branch for 2p emission from ^{63}Se cannot be excluded, the next more exotic isotope, ^{62}Se, is expected to emit two protons too fast, on the scale of 10 ns, and to have a cross section too small (less than 0.1 fb) for a meaningful experiment using projectile fragmentation of a ^{78}Kr beam. For ^{59}Ge, the 2p decay branch appears to be negligible, in agreement with findings of Ref. [7]. For ^{58}Ge we predict that it can be produced with ^{78}Kr beam with a cross section of about 0.8 fb and the rough prediction of its 2p-decay half-life points to a few hundreds of nanoseconds. The search for ^{58}Ge in Ref. [16] yielded, however, negative result suggesting a half-life limit of about 100 ns. In any case, a further search for a small branch of 2p radioactivity in ^{63}Se and a more discerning insight into the decay of ^{58}Ge will require measurements with larger beam intensity, providing higher statistical significance. Hopefully, conditions for such studies will be reached in the upcoming fragmentation facilities FRIB and FAIR.

ACKNOWLEDGMENTS

We would like to thank the whole RIBF accelerator staff for the support during the experiment and for maintaining excellent beam conditions.

This work was partially supported by the National Science Center, Poland, under Contracts No. UMO-2015/17/B/ST2/00581 and 2019/33/B/ST2/02908, by the University of Warsaw Integrated Development Programme (ZIP), co-financed by European Social Fund within Knowledge Education Development Programme 2014-2020, p.3.5, by the U.S. National Science Foundation under Grant No. PHY-2012040, by the Office of Nuclear Physics, U.S. Department of Energy under Award No. DE-FG02-96ER40983 (UTK), by the National Nuclear Security Administration under the Stewardship Science Academic Alliances program through DOE Award No. DE-NA0003899, and by the MEXT/JSPS KAKENHI grants No. 16K05390, 18H03602, and 18H05462.

[1] M. Pfützner, M. Karny, L.V. Grigorenko, and K. Riisager, Rev. Mod. Phys. **84**, 567 (2012).
[2] B. Blank and M.J.G. Borge, Progress in Particle and Nuclear Physics **60**, 403 (2008).
[3] H. Schatz et al., Phys. Rep. **294**, 167 (1998).
[4] L.V. Grigorenko et al., Phys. Lett. B **677**, 30 (2009).
[5] M. Pomorski et al., Phys. Rev. C **83**, 061303(R) (2011).
[6] B. Blank et al., Phys. Rev. Lett. **94**, 232501 (2005).
[7] T. Goigoux et al., Phys. Rev. Lett. **117**, 162501 (2016).
[8] E. Olsen et al., Phys. Rev. Lett. **110**, 222501 (2013); Phys. Rev. Lett. **111**, 139903 (2013).
[9] L. Neufcourt et al., Phys. Rev. C **101**, 014319 (2020).
[10] B. Blank et al., Phys Rev. Lett. **84**, 1116 (2000).
[11] C. Dossat et al., Phys. Rev. C **72**, 054315 (2005).
[12] M. Pomorski et al., Phys. Rev. C **90**, 014311 (2014).
[13] P. Ascher et al., Phys. Rev. Lett. **107**, 102502 (2011).
[14] A. Stolz et al., Phys. Lett. B **627**, 32 (2005).
[15] A.A. Ciemny et al., Phys. Rev. C **92**, 014622 (2015).
[16] B. Blank et al., Phys. Rev. C **93**, 061301(R) (2016).
[17] T. Kubo, Nucl. Instrum. Methods B **204**, 97 (2003).
[18] T. Kubo et al., Prog. Theor. Exp. Phys. **2012**, 03C003 (2012).
[19] N. Fukuda et al., Nucl. Instrum. Methods B **317**, 323 (2013)
[20] O.B. Tarasov and D.Bazin, Nucl. Instrum. Methods B **376**, 185 (2016); http://lise.nscl.msu.edu .
[21] J. Giovinazzo. et al., Eur. Phys. J. A 11, 247 (2001).
[22] K. Sümmerer, Phys. Rev. C **86**, 014601 (2012).
[23] `http://lise.nscl.msu.edu/AA`
[24] J.W.Wilson, L.W.Towsend, F.F.Badavi, Nucl. Instrum. Methods B **18** , 225 (1987).
[25] J.Gosset et al., Phys. Rev. C **16**, 629 (1977).
[26] O.B. Tarasov, D. Bazin, Nucl. Instrum. Methods B **204**, 174 (2003).
[27] X. Campi, J. Hüfner, Phys. Rev. C **24**, 2199 (1981).
[28] J.-J. Gaimard and K.-H. Schmidt, Nucl. Phys. A **531**, 709 (1991).
[29] A.S. Iljinov et al., Nucl. Phys. A **543**, 517 (1992).
[30] O.B. Tarasov, A.C.C.Villari, Nucl. Instrum. Methods B **266**, 4670 (2008).
[31] D. Bazin, B. Sherrill, Phys. Rev. E **50**, 4017 (1994).
[32] `http://users.ics.forth.gr/~lourakis/levmar`
[33] M. Wang, G. Audi, F.G. Kondev, W.J. Huang, S. Naimi, and X. Xu, Chin. Phys. C **41**, 030003 (2017).
[34] M. Wang, W.J. Huang, F.G. Kondev, G. Audi, and S. Naimi, Chin. Phys. C **45**, 030003 (2021).
[35] T. Tachibana, M. Uno, M. Yamada, and S. Yamada, At. Data Nucl. Data Tables 39, 251 (1988).
[36] H. Koura, T. Tachibana, M. Uno, and M. Yamada, Prog. Theor. Phys. 113, 305 (2005).
[37] P. Möller, W.D. Myers, H. Sagawa, and S. Yoshida, Phys. Rev. Lett. **108**, 052501 (2012).
[38] N. Wang, M. Liu, X. Wu, and J. Meng, Phys. Lett. B **734**, 215 (2014).
[39] S. Goriely, N. Chamel, and J. M. Pearson, Phys. Rev. C 88, 024308 (2013).
[40] S. Goriely, N. Chamel, and J. M. Pearson, Phys. Rev. C 88, 061302(R) (2013).
[41] M. Kortelainen, T. Lesinski, J. More, W. Nazarewicz, J. Sarich, N. Schunck, M.V. Stoitsov, and S. Wild, Phys. Rev. C **82**, 024313 (2010).
[42] M. Kortelainen, J. McDonnell, W. Nazarewicz, P.-G. Reinhard, J. Sarich, N. Schunck, M. V. Stoitsov, and S.M. Wild, Phys. Rev. C **85**, 024304 (2012).

[43] M. Pfützner, Phys. Scr. **T152**, 014014 (2013).